Appl. Phys. B 52, 217–224 (1991)

Applied Physics B Photophysics and Laser Chemistry

Measurement of Er:YAG Laser Ablation Plume Dynamics*

J. T. Walsh, Jr. and T. F. Deutsch**

Wellman Laboratories of Photomedicine, Department of Dermatology, Massachusetts General Hospital, Boston, MA 02114, USA

Received 4 October 1990/Accepted 15 October 1990

Abstract. The dynamics of tissue ablation using an Er:YAG laser were studied using flash photography and optical pump-probe techniques. Both normal-spiking-mode and Q-switched Er:YAG laser radiation were used to study the ablation of skin and bone. Time-resolved photographs of the ablation plume were obtained using a microscope-mounted camera together with pulsed illumination from an excimer-pumped dye laser. The velocity of the plume front, obtained from the photographs, was approximately 1400 m/s. The same velocity was also measured using an optical pump-probe technique. Both techniques indicate that material removal occurred after the end of the 90-ns-long Q-switched laser pulse and that each micropulse in the normal-spiking-mode pulse train was capable of ablating and rapidly ejecting tissue.

PACS: 87.60Gp

Tissue ablation using pulsed infrared lasers is being investigated because these lasers typically produce surgical cuts with less damage than continuous-wave lasers [1]. Experimentation with pulsed infrared lasers has led to an interest in modeling the ablation process. Simple static thermal models of laser ablation of tissue are useful for understanding basic ablation parameters such as tissue removal efficiency and threshold fluence for ablation. It is, however, generally understood that ablation is a complex dynamic explosive process. Thus, studies of the dynamics of tissue ablation can be useful in evaluating models of tissue ablation by determining quantities such as the time delay between laser irradiation and tissue removal, the velocity of the ablated material, and the duration of post-pulse ablation. In addition, issues that may impact the clinical usefulness of the laser-ablation process may be identified. For example, shadow photography can demonstrate the existence of potentially destructive shock waves. The Er:YAG laser, emitting 2.94-μm radiation, has been of interest as a potential surgical tool because its output wavelength corresponds with the peak of the liquid water absorption band. Studies have shown that the Er:YAG laser can readily ablate both soft and hard tissue, leaving between 5 and 100 μm of damaged tissue at the cut edge [1–5]. Models applicable to mid-infrared laser ablation have been proposed [6–9]. Each of these models makes predictions about the temporal and spatial duration of the ablation plume. An analysis of the dynamics of the ablation process should yield a more complete understanding of mid-infrared laser ablation of tissue and allow the development of more accurate ablation models.

The explosive nature of pulsed-laser ablation was first described by Ready in 1963 [10]. Theoretical models and their experimental verification in ceramics occurred a decade later [6, 11]. Although the plume produced by mid-infrared laser radiation has not been photographed previously, several investigators have photographed the plume produced by radiation from other lasers. Recently, a number of researchers have used flash photography to study ablation of biological materials. Prince et al. have shown that 1-μs-long pulses of 459–470 nm light can cause explosive removal of biological materials and that ablation continues for at least 150 μs after the pulse [12]. Puliafito et al. have shown that UV laser ablation of cornea results in rapid ejection of material [13]. In this latter study, the velocity and size of the ejected particles were found to be dependent upon the optical penetration depth of the incident radiation. More recently, Zweig et al. have used high-speed photography to demonstrate that

* This work was supported in part by the SDIO-MFEL Program under contract # N00014-86-K-0117 and by the Arthur O. and Gullan M. Wellman Foundation

** Permanent address: Biomedical Engineering Department, Northwestern University, 2145 Sheridan Road, Evanston, IL 60208-3107, (708)-491-7118 (office), (708)-491-5299 (FAX)

mechanical deformation of a tissue phantom, gelatin, is influenced by focusing conditions and by the temporal profile of the pulse [5].

We studied the dynamics of the plume of material ejected from the tissue surface using two methods: an optical pump-probe technique and flash microphotography. Both methods allowed measurement of the plume front velocity by using data from the first few hundred nanoseconds after the 90-ns-long ablative pulse. The optical pump-probe technique gave information about the effect of each micropulse in the normal-spiking-mode pulse train. The flash microphotography method yielded additional information about particle size and the existence of shock waves in air. The experimental and theoretical study of the propagation of shock waves is extensive [14–18] and considers the evolution from 1) an initial mass-dependent regime, to 2) a strong shock (or blast wave) regime, to 3) the eventual deceleration of the shock wave to acoustic velocities. We have analyzed our data in the context of the existing shock wave models.

1. Materials and Methods

1.1. Flash Microphotography

The plume produced during the Er:YAG laser ablation of both soft and hard tissue was photographically recorded. The soft tissue was Caucasian cadaver abdominal skin obtained from autopsy, refrigerated and used within 60 hours post-mortem. The hard tissue was guinea pig parietal bone (Hartley strain) that was obtained from freshly sacrificed animals; the parietal bone was exposed and the periosteum removed from both the extracranial and intracranial surfaces.

The 2.94-μm radiation from an Er:YAG laser (Schwartz Electro-Optics) was focused with an 20-cm-focal-length, plano-convex BaF_2 lens onto the surface of the tissue (Fig. 1). Flash photographs were taken with the laser operating in both the normal-spiking mode, where the output was a series of approximately twenty 1-μs-long micropulses in a 250-μs-long macropulse envelope, and in the Q-switched mode, where a single 90-ns-long (FWHM, full-width half-maximum) pulse was emitted. A 6-mm-diameter punch biopsy of skin was placed inside a plastic holder so that the skin surface was normal to the incident laser radiation. The bone was held with a clamp and positioned so that the irradiated surface was normal to the incident beam. The tissues were carefully positioned with an X–Y–Z translator to be at the focus of the 20-cm-focal-length lens *and* at the focus of a stereomicroscope. The microscope was equipped with a photoextension tube and a 35-mm camera. The optical axis of the microscope was parallel to the optical table and normal to the axis of the incident 2.94-μm beam. The source of illuminating light was an excimer-pumped dye laser emitting a nominally 20-ns-long (FWHM) pulse of 632-nm light. Between 1.2 and 1.4 mJ of illumination light was emitted from a 1-mm-core-diameter fiber positioned for shadow photography. A 632-nm bandpass filter was placed in the microscope photoextension tube before the camera in order to avoid exposing the film with the white light from the laser flashlamp.

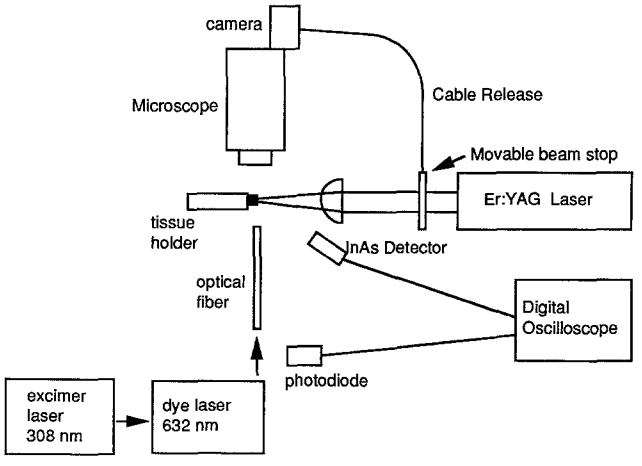

Fig. 1. Schematic diagram of the apparatus used to photographically record the Er:YAG laser-induced ablation plume (top view)

Synchronization of the Er:YAG laser pulse and the illuminating pulse was achieved by passing the "sync-out" pulse from the Er:YAG laser power supply through an electronic variable-delay circuit (Tektronix oscilloscope model 7834 with timebase 7B92) to the excimer laser trigger. The delay circuit allowed illumination at times from approximately 1 μs before to greater than 1 ms after arrival of the ablative pulse. With the Er:YAG laser operating in the Q-switched mode synchronization was difficult because it was necessary to record within 1 μs after the beginning of the 90-ns-long Q-switched pulse. However, the jitter between the Q-switched pulse and the "sync out" pulse was ± 3 μs. Such jitter is expected from a rotating mirror Q-switch. Photographs of the ablation plume emanating from the skin, which occurs from 0.25 to 3 μs after the laser pulses, were obtained with difficulty. Bone ablation was not photographed in Q-switched mode because of the difficulty in obtaining data in the 1 ns to 1 μs time-delay range over which bone ablation occurred.

The time between the ablative pulse and the illuminating pulse was measured using a digital oscilloscope (LeCroy model 9400). The 2.94-μm radiation scattered from the tissue surface was detected by an InAs detector (Judson Infrared, Inc, model J12-LD-R250U, rise time ≈ 50 ns). The 632-nm light was detected by a fast Si photodiode. The delay time was measured from the beginning of the ablative pulse to the beginning of the illuminating pulse.

The ablation plume was photographed in a darkened room with both the Er:YAG laser and the illuminating laser operating at 1 Hz. A beam stop blocked the 2.94-μm radiation. When the beam stop was moved a single Er:YAG laser pulse struck the tissue and a single 632-nm pulse illuminated the plume and exposed the film.

The energy of the incident 2.94-μm radiation was determined using a joulemeter (Gentec ED-200). The diameter of the irradiated spot was determined from the crater produced on the surface of a piece of paper, a procedure that has been independently shown to yield

spot diameters nearly identical to those determined by scanning a 10-μm-diameter pinhole through the focus [19]. For all Q-switched experiments the spot diameter was 350 μm ($1/e^2$ points) and the energy per pulse was 25 ± 5 mJ/pulse. The average fluence was thus approximately 26 J/cm^2. For all normal-spiking-mode irradiations the beam was uniform to $\pm 10\%$ and had a spot diameter of 1.1 mm at the half maximum points [19]. The energy was 500 ± 5 mJ/pulse, resulting in a fluence of approximately 53 J/cm^2.

1.2. Optical Pump-probe Measurements

Figure 2 shows the pump-probe system. The 2.94-μm radiation from the Er:YAG laser was again focused onto the surface of the tissue with an 20-cm-focal-length, BaF_2 lens. The 632-nm light from a HeNe laser was expanded by 8X and then focused with a 12-cm-focal length lens to achieve a 90-μm diameter beam ($1/e^2$ points) that passed immediately in front of the target tissue. The depth of field (the distance over which the beam diameter changes by $\pm 5\%$) at the focus was measured to be 3 mm. This depth of field was considered adequate given the 1.1-mm-diameter spot irradiated by the normal-spiking-mode Er:YAG laser and the 350-μm diameter spot irradiated in the Q-switched mode. After passing the tissue, the HeNe beam was refocused onto a fast Si photodiode with an approximately 1-ns rise time. A 632-nm bandpass filter was placed in front of the photodiode to block any stray radiation. A InAs detector with a 50-ns rise time was again used to detect scattered 2.94-μm radiation. The signals from both the InAs detector and the photodiode were recorded with a digital oscilloscope. When a pulse from the Er:YAG laser struck the tissue, a plume developed. The plume traveled a known distance from the tissue surface into the focus of the HeNe beam. Interruption of the HeNe beam was detected by the Si photodiode. Simultaneous recording of the signals allowed measurement of the time between the Er:YAG laser pulse and the interruptions of the probe beam.

A 6-mm-diameter punch biopsy of skin was placed inside a plastic holder with the skin surface normal to the incident Er:YAG laser beam. The tissue surface was carefully positioned with an X–Y–Z translator to be at the focus of the Er:YAG laser beam and at the focus of the HeNe laser beam. Because the depth of field of the Er:YAG laser beam is several millimeters, the calibrated X–Y–Z translator could be used to move the tissue surface a short (i.e., less than 1 mm) distance back from the HeNe beam. As with the flash photography, the time delay was measured from the beginning of the rise of the 2.94-μm pulse to the beginning of the change in the 632-nm signal.

Q-switched, the fluence was varied from 2.5 to 24 J/cm^2. Normal-mode the fluence was varied from 7.5 to 42 J/cm^2. The distance between the tissue surface and the focus of the HeNe beam was varied from 100 to 1000 μm.

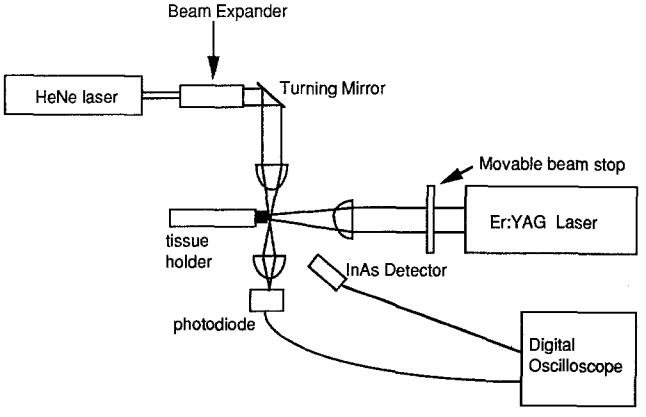

Fig. 2. Schematic diagram of the optical pump-probe set-up used to investigate the dynamics of the Er:YAG laser ablation of tissue (top view)

2. Results

Figure 3 shows a series of photographs illustrating the Q-switched Er:YAG laser ablation of human skin. Of the 377 photographs of Q-switched Er:YAG laser ablation of skin, 169 of them showed ablation plumes. Most of the negatives that did not show a plume were exposed either before the ablation pulse arrived or long enough after the ablation pulse that no plume material remained in the field of view. No ablation plume was observed until 250 ns after the beginning of the 90-ns-long (FWHM) Q-switched pulse. Thus, we find no plume ejection during the Q-switched pulse. The photographs indicate that initially a dense cloud of material rapidly leaves the tissue surface. Within this cloud particles larger than 20 μm are not evident; at later times, however, particles 20–50 μm in size are seen, e.g. see the 3.54-μs time-delay photograph. As time progresses the plume front, which consists of particles, will fall behind and separate from the shock front, which consists of a surface across which there is a pressure discontinuity. This phenomenon is observed in some of the photographs in which a smooth curve is seen ahead of the plume front. The smooth curve is caused by the change in refractive index across the shock front. Note that for time delays greater than 980 ns, although the ejection of material from the surface was clearly evident, the plume front had moved beyond the field of view of the microscope.

Figure 4a shows the position of the plume front, which is expected to coincide with the shock front at early times, versus time; Figure 4b shows the position of the shock front observed ahead of the plume front in some of the photographs. A logarithmic representation is used to facilitate comparison with the behavior of ideal strong shocks, considered in the discussion section below. A linear representation was used, in combination with extrapolation of a least-squares linear regression, to determine the time between the beginning of the laser pulse and when material began to leave the tissue surface. This delay time was 281 ns (95% confidence interval 77–385 ns). Because the delay time is obtained by extrapolation, observations very close to the target surface are not required to accurately determine the delay time. From the linear representation of the plume front and shock

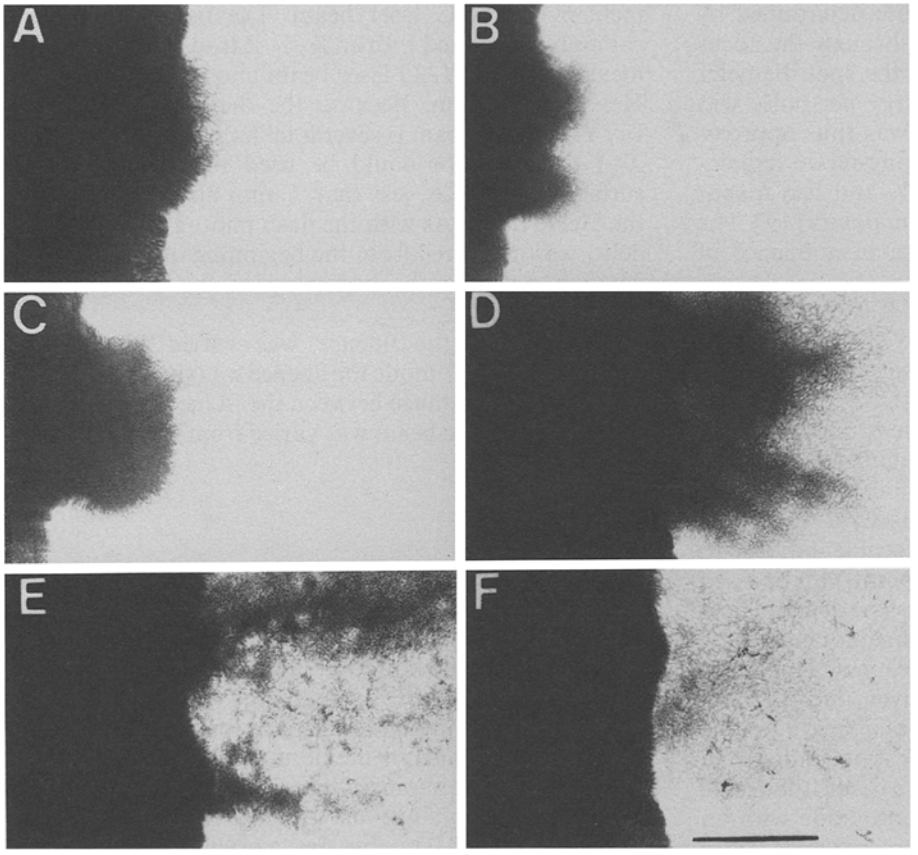

Fig. 3A–F. Flash photomicrographs of the ablation plume produced by a 26 J/cm^2, 90-ns-long (FWHM), Q-switched Er:YAG laser pulse incident on human dermis. Each photograph is for a different laser pulse. The time from the beginning of the macropulse is **A** 300 ns, **B** 480 ns, **C** 700 ns, **D** 1.13 μs, **E** 2.66 μs, **F** 3.54 μs. No plume was ever noted for time delays of less than 250 ns · bar = 500 μm

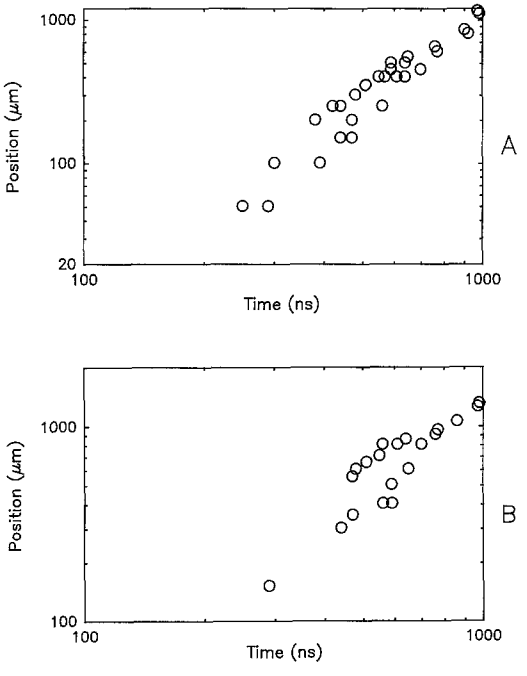

Fig. 4. A Position of the particle front versus time after the beginning of the Q-switched Er:YAG laser pulse. **B** Position of the shock front versus time after the beginning of the Q-switched Er:YAG laser pulse. The time delay between the beginning of the ablation and illumination pulses was determined from the oscilloscope tracing. The distance the front had moved from the dermal surface was determined from the photographs

front data one finds that the mean velocity of the plume front was 1413 ± 78 m/s (mean ± standard error) while that of the shock front was 1615 ± 168 m/s (mean ± standard error). One should note that the speed of sound in air is 344 m/s (at 1 atmosphere pressure, 20°C, and 100% relative humidity [20]).

Figure 5 shows a series of photographs illustrating the normal-spiking-mode Er:YAG laser ablation of human dermis. After one micropulse, 2.5 μs after the beginning of the macropulse, a plume is evident. In the middle of the macropulse (65–165 μs) considerable material removal is evident. Even after the macropulse is over, 315 μs after the beginning of the macropulse and 90 μs after the end of the macropulse, ejection of material is clearly evident. The 1-ms photograph indicates plume material near the tissue but ablation no longer appears to be occurring. The photographs at approximately 65 and 92 μs indicate intermittent ejection of more dense clouds of material. From the photographs alone it is not possible to determine if these "packets" were ejected by an individual micropulse or if intermittent ejection would occur even if the macropulse had a temporally constant intensity. Determination of plume velocity was not possible because the plume front rapidly moved beyond the microscope's field of view.

Figure 6 shows a series of photographs illustrating the normal-spiking-mode Er:YAG laser ablation of guinea pig parietal bone. After one micropulse, 5.8 μs after the

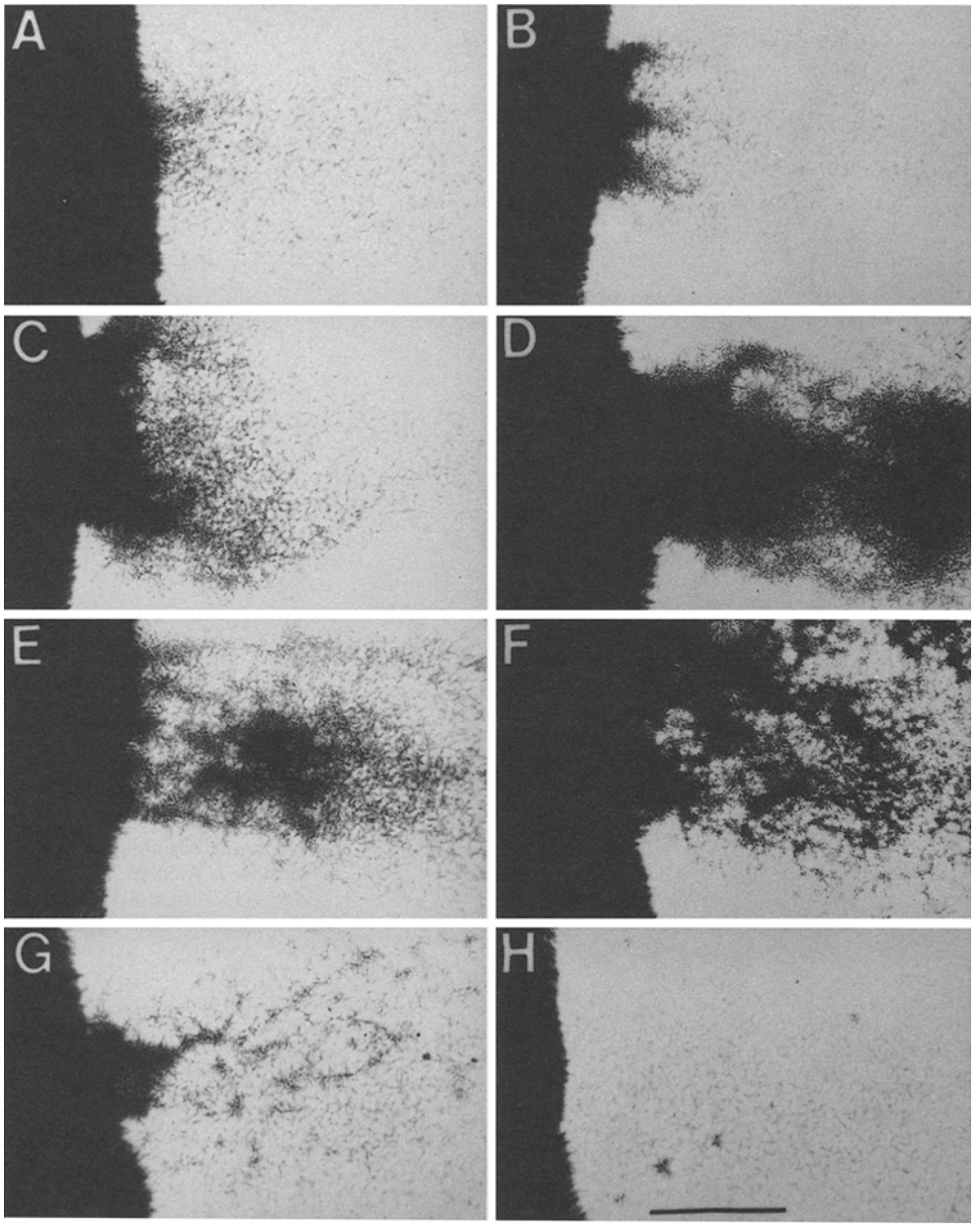

Fig. 5A–H. Flash photomicrographs of the ablation plume produced by a 53 J/cm^2, normal-spiking-mode Er:YAG laser pulse incident on human dermis. Each photograph is for a different laser pulse. The time from the beginning of the macropulse is **A** 2.5 μs, **B** 9.9 μs, **C** 25.2 μs, **D** 65.2 μs, **E** 91.7 μs, **F** 165.7 μs, **G** 316 μs, **H** 1 ms · bar = 500 μm

beginning of the macropulse, a plume is evident. In the middle of the macropulse (36–116 μs) considerable material removal is evident. However, after the macropulse no further ejection of material was seen. Thus, it appears that, unlike the ablation of soft tissue which continued after the ablation pulse, the ablation of hard tissue ends at approximately the same time as the ablation pulse. Further, the photographs give the impression that the bone plumes are composed of larger, more discrete material than was seen in the dense cloud of material produced in the dermis plumes.

The velocity of the plume created by a Q-switched Er:YAG laser pulse was also measured using an optical pump-probe technique. The pump-probe measurements give the time at which the particle front passes and blocks the beam; the detection geometry was not sensitive enough to detect the passage of the shock front, which only deflected the probe beam slightly. Figure 7 shows logarithmic representation of plume front position versus time for three different fluences. A linear representation of the 24 J/cm^2 data indicates that the velocity of the plume front is 1327 m/s (95% confidence interval: 1154–1553 m/s) and that the plume first leaves the tissue surface 94 ± 40 ns (mean ± standard error) after the start of the Q-switch pulse. Both of these values are in reasonable agreement with the flash photography data. Figure 8 shows a typical oscilloscope trace for a normal-spiking-mode pulse. Note that each micropulse appears to eject a separate bolus of tissue from the surface.

3. Discussion

Two methods were used to investigate the dynamics of the Er:YAG laser ablation of tissue. For the ablation of dermis with a Q-switched Er:YAG laser both methods

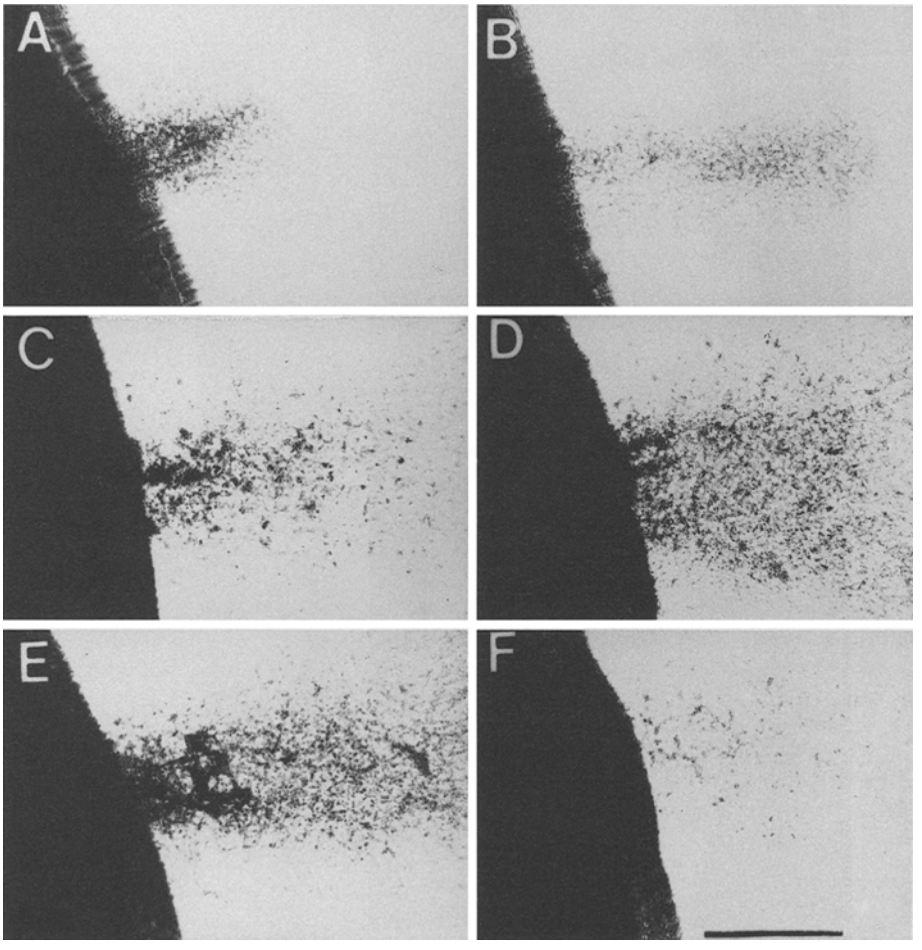

Fig. 6A–F. Flash photomicrographs of the ablation plume produced by a 53 J/cm^2, normal-spiking-mode Er:YAG laser pulse incident on guinea pig parietal bone. Each photograph is for a different laser pulse. The time from the beginning of the macropulse is **A** 5.8 μs, **B** 13.4 μs, **C** 36.6 μs, **D** 77.6 μs, **E** 116 μs, **F** 207 μs · bar = 500 μm

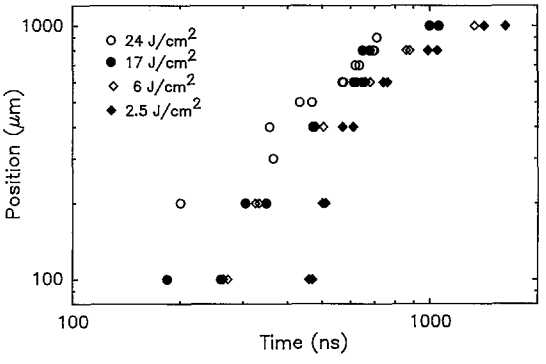

Fig. 7. Position of the particle front versus the time after the beginning of the Q-switched Er:YAG laser pulse. The distance from the dermal surface to the HeNe beam focus was known from the setting of the micrometer used to position the tissue. The time delay between the beginning of the ablation pulse and the interruption of the HeNe laser beam was determined from the oscilloscope tracing

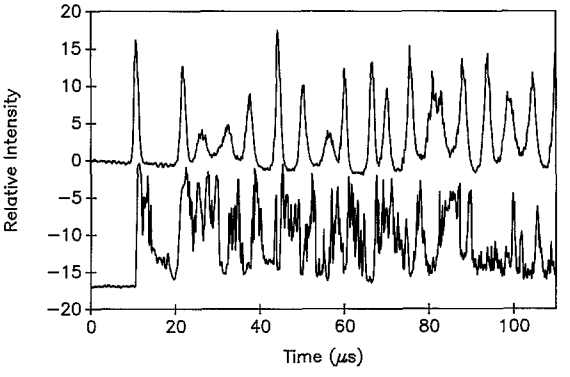

Fig. 8. Typical oscilloscope trace obtained using the optical pump-probe technique to investigate the normal-spiking-mode Er:YAG laser ablation plume. The distance from the dermal surface to the focus of the HeNe beam was 100 μm. The fluence per pulse was 42 J/cm^2. Note the nearly one-to-one correspondence between the Er:YAG laser micropulses (upper trace) and the interruption of the HeNe beam (lower trace)

indicate that the plume does not start to leave the tissue surface until near the end of or after the 90-ns-long (FWHM) pulse. Furthermore, there appears to be considerable ejection of material for several microseconds after the pulse. The velocity of the plume front, as determined from both the flash photography data and the pump-probe data, is greater than 4 times the speed of sound in air. Flash photography reveals the presence of shock waves in front of the plume.

The evidence gathered in this study is consistent with an explosive model for the Er:YAG laser ablation of tissue [8, 9, 19]. The incident radiation is strongly absorbed by the water in tissue. The water heats rapidly, vaporizes and expands. A simple calculation shows that

only about 1% of an incident 25 J/cm^2 pulse is necessary to provide the 2.5 kJ/cm^3 needed to vaporize the water in a surface layer one optical absorption length (about 1 μm) thick. Thus vaporization should occur early on during the pulse; our measurement systems, however, would probably not detect water vaporization. We do not see tissue leaving the surface until after the entire pulse is over. This may be because it takes time for the confined water vapor to expand, for the bone or tissue matrix that maintains the structural integrity of the tissue to break, and for the tissue to accelerate away from the surface. Studies of pulsed CO_2 laser ablation of a variety of tissues showed that the ablation efficiency was strongly dependent upon the mechanical properties of the tissue [21]. Thus, the confinement time may also be a function of the mechanical properties of the tissue. A more detailed investigation of Q-switched laser ablation of tissues with different mechanical properties may confirm this hypothesis.

The delayed ejection of tissue may have an effect on the residual damage at the ablation crater edge. In particular, if the hot vapor does not leave the tissue surface for several microseconds, then considerable transfer of thermal energy into the nonablated tissue can occur. Such heat transfer from hot vapor could lead to nonablated tissue thermally damaged to depths greater than the optical penetration depth of the incident 2.9-μm radiation, as has been observed [3, 9, 22, 23]. However, recent work has provided evidence that a reservoir of liquefied material around the walls of the crater mediates the thermal damage [24, 25]. In addition, during the time between the end of the pulse and the onset of ablation, subsurface expansion of water vapor may lead to tears or vacuoles at the edges of a cut; such tears have been observed in the Er:YAG laser ablation of cornea [9].

Analysis of the flash photographs of ablation of skin showed the existence of a plume front, preceded by a shock front, with both fronts moving at supersonic velocity. The shock wave is launched by the rapid explosive ablation of material. The shock wave separates from the plume front in a manner similar to the way a laser-induced plasma in water launches a shock wave that propagates beyond the plasma [26]. Figures 4a and b depict the dependence of position of the plume front and the shock front on time indicating that the front velocities are constant. The data of Fig. 7 show a superlinear time dependence, i.e. the front velocity increases with time and the front position goes as $t^{1.1}$ to $t^{1.6}$. These results appear to be in conflict with the theory describing the propagation of strong shocks (blast waves) in air. Sedov has predicted the motion of the shock front caused by an intense explosion for spherical and plane waves [14]. The dependence of the position of the shock front, r, on time, t, is given by

$$r=(E/\varrho_0)t^{0.4} \quad \text{for a spherical shock} \tag{1a}$$

and

$$r=(E/\varrho_0)t^{0.67} \quad \text{for a planar shock}, \tag{1b}$$

where E is the energy released by the explosion, and ϱ_0 is the density of the gas in front of the shock. Position is measured from the origin of the explosion. The geometry of our set-up suggests that the shape of the plume front might better be described as planar rather than spherical; the shape of the actual shock wave is, however, spherical.

The apparent disagreement of our data with the theory can be understood by considering the range of distance over which the model of strong shocks is expected to be valid. This range has been considered by several authors [16–18]. The theory requires that the explosion mass, M, be small compared to the mass of the gas enclosed by the shock wave. This can be expressed as [18]

$$r \gg R=(3M/2\pi\varrho_0)^{1/3}. \tag{2}$$

We can evaluate R for our experiment using as M the mass of tissue ablated in a pulse. We used a Q-switched Er:YAG laser emitting 25 mJ/pulse to irradiate a 350 μm diameter spot. Using a previously measured ablation efficiency of 0.54 mg/J [19] one calculates that 0.014 mg of tissue was ablated per pulse. Using an air density of 1.25 mg/cm^3, one calculates $R=1.7$ mm. Thus the range of our observations, $r=0.1$–1 mm, was too close to the origin to apply the classical Taylor-Sedov strong shock model. Instead our data was taken in the mass-dependent flow regime. Freiwald and Axford obtained an analytic solution to shock front motion in this regime [17]. We have applied this model to the data in Fig. 4b. The data and the theory show the same general trends, however, adequate fitting of the data is not possible without seemingly indiscriminate selection of the various independent model parameters. As Leonard and Hammerling have suggested, precise knowledge of M (the mass ablated) and γ (the specific heat ratio of the ambient gas), both of which may change dynamically during the time of interest, is necessary in order to calculate the energy, E, of the expanding shock wave in the mass-dependent regime [16].

Our results can be compared with those of several other studies. Dyer and Sidhu measured the motion of the luminous fronts observed in 308-nm excimer laser ablation of polyimide and found a transition from mass-dependent to classical Taylor-Sedov strong shock behavior as the ablation front developed [18]. Behavior close to that of an ideal strong shock can be found upon reanalysis of published flash photographic studies of ablation. The measurements by Puliafito et al. on corneal ablation [13], give a $t^{0.35}$ dependence; similarly the flash photographs of PMMA ablation taken by Srinivasan et al. show a shock wave whose position depends on $t^{0.67}$ [27]. The accuracy of our analysis is limited because of the small number of data points; nevertheless, the analysis indicates that under appropriate condition classical strong shock behavior is observed using flash photography methods. A larger set of data would allow the determination of the portion of the absorbed energy that is converted into kinetic energy, i.e. E in (1a and 1b).

The effect of shock waves in air may be deleterious if ablation is conducted in a confined space near sensitive organs, in the middle ear, for example. Rapid particle ejection may also induce shock waves in the nonablated tissue [28, 29]. Shock waves induced by ArF-excimer-

laser ablation of skin have been postulated as the cause of damage to organelles several hundred micrometers below the surface of the skin [30]; the clinical significance of such damage remains to be determined. Er:YAG laser-induced shock waves in tissue may also damage structures distant from the site of irradiation. Further investigation of the existence of shock waves in tissue is warranted, as is the investigation of shockwave-induced damage.

The results of the normal-spiking-mode Er:YAG laser ablation study indicate that some important differences exist between the ablation of "soft" and "hard" tissues. The material ejected from the bone surface clearly contained discrete particles; the material ejected from the skin surface was more reminiscent of a continuous cloud. The higher water content of the skin may be responsible for this. The ejection of material from the bone surface ceases at the end of the laser pulse train; the ejection of material has been predicted by modeling. A thin layer of 100 μs after the end of the pulse. Post-pulse ablation of material has been predicted by modelling. A thin layer of tissue near the critical temperature of water is present at the base of the ablation crater [7]. Because of ablative cooling at the bottom of the crater, the peak in the spatial temperature profile is below the bottom of the crater [6]. This heated tissue can be ablated after the laser pulse if sufficient energy is available to drive vaporization or if the pressures present within the tissue exceed the breaking strength of the tissue. For skin, which is typically 70% water, both of these ablation processes probably occur. For bone, which is typically 10% water, the ablation process is, however, likely to be solely an explosive process. The pressures for explosive ablation of bone are expected to be higher than those for explosive ablation of skin and are apparently reached only during the laser pulse.

For the normal-spiking-mode Er:YAG laser ablation of tissue both methods indicate that each micropulse ejects a separate bolus of tissue and that material ejection ceases between micropulses. This is probably the result of both the fluences we used and the fact that the typical time between micropulses, 5–10 μs, is several times the 1-μs relaxation time of the 1-μm-thick laser heated volume. Thus cooling between pulses can be significant. At fluences in which the energy in each micropulse is insufficient to reach the ablation threshold, then ablative cooling of the tissue would not occur and one would expect to see a accumulation of the energy from separate micropulses. Such summation effects have been observed in framing camera studies of tissue ablation using a pulsed Ho:YAG laser emitting at 2.1-μm, where the absorption coefficient of water is small [31]. Thus both the fluences used and the diffusion of heat between micropulses will generally have to be considered in understanding the dynamics of ablation.

In summary, we have shown that the ablation dynamics of bone and dermis by the Er:YAG laser depend on the target tissue and involve the ejection of material at supersonic velocities, as well as generation of shock waves in air. Further studies are needed to understand the effect of these processes on mechanical and thermal damage to the target tissue.

Acknowledgements. We gratefully acknowledge the technical assistance of F. Long, V. Natoli, and P. Teng at various stages of this work. We thank F. Hillenkamp, and D. Rosen for numerous technical discussions and J. A. Parrish for his interest in and support of this project.

References

1. M.L. Wolbarsht: IEEE J. QE-**20**, 1427–1432 (1984)
2. R.F. Bonner, P.D. Smith, M. Leon, L. Esterowitz, M. Strom, K. Levin, D. Tran: Proc. SPIE **713**, 2–5 (1986)
3. J.S. Nelson, L. Yow, L.H. Liaw, L. Macleay, R.B. Zavar, A. Orenstein, W.H. Wright, J.J. Andrews, M.B. Berns: Lasers Surg. Med. **8**, 494–500 (1988)
4. J.T. Walsh, T.J. Flotte, T.F. Deutsch: Lasers Surg. Med. **9**, 314–325 (1989)
5. A.D. Zweig, M. Frenz, V. Romano, H.P. Weber: Appl. Phys. B **47**, 259–265 (1988)
6. F.U. Dabby, U.C. Paek: IEEE J. QE-**8**, 106–111 (1972)
7. D.I. Rosen, L.A. Popper: Proc. SPIE **1064**, 30–39 (1989)
8. A.D. Zweig, H.P. Weber: IEEE J. QE-**23**, 1787–1793 (1987)
9. J.T. Walsh, T.F. Deutsch: Lasers Surg. Med. **8**, 264–275 (1988)
10. J.F. Ready: Appl. Phys. Lett. **3**, 11–13 (1963)
11. U.C. Paek, V.J. Zaleckas: Ceram. Bull. **54**, 585–588 (1975)
12. M.R. Prince, T.F. Deutsch, A.H. Shapiro, R.J. Margolis, A.R. Oseroff, J.T. Fallon, J.A. Parrish, R.R. Anderson: Proc. Natl. Acad. Sci., USA **83**, 7064–7068 (1986)
13. C.A. Puliafito, D. Stern, R.R. Krueger, E.R. Mandel: Arch. Ophthalmology **105**, 1255–1259 (1988)
14. L. Sedov: *Similarity and Dimensional Methods in Mechanics* (Academic, New York 1959)
15. Ya.B. Zel'dovich, Yu.P. Raizer: *Physics of Shock Waves and High Temperature Hydrodynamic Phenomena* (Academic, New York 1966)
16. T.A. Leonard, P. Hammerling: J. Appl. Phys. **51**, 6130–6133 (1980)
17. D.A. Freiwald, R.A. Axford: J. Appl. Phys. **46**, 1171–1174 (1976)
18. P.E. Dyer, J. Sidhu: J. Appl. Phys. **64**, 4657–4663 (1988)
19. J.T. Walsh, T.F. Deutsch: Lasers Surg. Med. **9**, 327–337 (1989)
20. R.C. Weast, M.J. Astle (eds.): *CRC Handbook of Chemistry and Physics*, 60th edn. (CRC Press, Boca Raton, FL 1979) p. E-53
21. J.T. Walsh, T.F. Deutsch: IEEE Trans. BE-**36**, 1195–1201 (1989)
22. D. Stern, C.A. Puliafito, E.T. Dobi, W.I. Reidy: Ophthalmology **95**, 1434–1441 (1988)
23. H. Loertscher, S. Mandelbaum, R.K. Parrish, J.M. Parel: Am. J. Ophthalmol. **102**, 217–221 (1986)
24. K.T. Schomacker, J.T. Walsh, J.T. Flotte, T.F. Deutsch: Lasers Surg. Med. **10**, 74–84 (1990)
25. A.D. Zweig, B. Meierhofer, O.M. Müller, C. Mischler, V. Romano, M. Frenz, H.P. Weber: Lasers Surg. Med. **10**, 262–274 (1990)
26. B. Zysset, J.G. Fujimoto, T.F. Deutsch: Appl. Phys. B **48**, 139–147 (1989)
27. R. Srinivasan, B. Braren, K.G. Casey, M. Yen: Appl. Phys. Lett. **55**, 2790–2792 (1989)
28. R. Srinivasan, P.E. Dyer, B. Braren: Lasers Surg. Med. **6**, 514–519 (1987)
29. R. Srinivasan: Science **234**, 559–565 (1986)
30. S. Wantanabe, J.T. Flotte, D.J. McAuliffe, S.L. Jacques: J. Invest. Dermatol. **90**, 761–766 (1988)
31. Y. Domankevitz, N. Nishioka: IEEE J. Quantum Electron. (in press)